Modeling of Regime Transition in Bubble Columns with Stability Condition

ARTICLE *in* INDUSTRIAL & ENGINEERING CHEMISTRY RESEARCH · JANUARY 2009

Impact Factor: 2.59 · DOI: 10.1021/ie8003623

4 AUTHORS, INCLUDING:

Ning Yang
Chinese Academy of Sciences
34 PUBLICATIONS **680** CITATIONS
SEE PROFILE

Wei Ge
Chinese Academy of Sciences
136 PUBLICATIONS **2,051** CITATIONS
SEE PROFILE

Modeling of Regime Transition in Bubble Columns with Stability Condition

Jianhua Chen,[†,‡] Ning Yang,*[,†] Wei Ge,[†] and Jinghai Li[†]

State Key Laboratory of Multi-Phase Complex Systems, Institute of Process Engineering, Chinese Academy of Sciences, P.O. Box 353, Beijing 100190, People's Republic of China and Graduate School of Chinese Academy of Sciences, Beijing 100039, People's Republic of China

Understanding the physical essence of regime transition is of crucial importance for the modeling and simulation of hydrodynamics and heat and mass transfer in bubble columns. The regime transition of the air−water system has been captured by the dual-bubble-size (DBS) model in our previous work [Yang et al. *Chem. Eng. Sci.* **2007**, *62*, 6978−6991] as a jump change from one minimum point of the stability criterion to the other. The DBS model features the incorporation of a stability condition with hydrodynamic conservation equations through the analysis of compromise between dominant mechanisms. This work reiterates our previous work and further explores some remaining issues and underlying physics related to the jump change by analyzing the trajectory of global minimum points in the three-dimensional space of structural parameters. The influence of drag coefficient correlations on the model prediction is investigated. The effect of liquid viscosity on regime transition is evaluated using the DBS model for saccharose and glycerin systems. The dual effects of liquid viscosity reported in literature, namely, suppressing the regime transition while slightly increasing viscosity and destabilizing the homogeneous regime at higher viscosity, can be reasonably predicted with this model. Finally, the concept of the compromise between dominant mechanisms is extended to understand the bubble behavior at different scales and its relationship with stability condition.

1. Introduction

Bubble columns have found widespread applications in chemical, biochemical, environmental, pharmaceutical, and petrochemical industries[1,2] due to the advantage of easy construction, lower energy consumption, and excellent mixing capability. Design and optimization of these processes requires an extensive understanding of the hydrodynamics of bubble column reactors, and particularly the so-called structural heterogeneity and regime multiplicity.[3]

A good deal of effort has been undertaken in the study of hydrodynamics and flow regimes by employing various experimental[4–9] techniques such as electrical resistance tomography (ERT),[10–12] electrical capacitance tomography (ECT),[13,14] computed automated radioactive particle tracking(CARPT)/computed tomography (CT),[15–17] particle image velocimetry (PIV),[18–20] magnetic resonance imaging(MRI),[21] and laser and phase Doppler anemometry(LDA, PDPA).[22–24] Generally speaking, the flow regimes in bubble columns can fall into three categories: homogeneous (bubbly), transition, and heterogeneous (churn-turbulent) flows. Homogeneous flow prevails at low gas flow rate with bubbles uniformly distributed and gas holdup increasing linearly with gas velocity, whereas the heterogeneous flow is pronounced at high gas flow rate and the linear relationship breaks down. Transition flow bridges the gap between the homogeneous and heterogeneous regimes, exhibiting the onset of bubble coalescence and breakup and thereby leading to inhomogeneous bubble size distribution and bulk liquid circulation. For example, Chen et al.[4] investigated macroscopic flow structures of 3-D bubble columns through PIV measurement. The flow regimes were identified as the dispersed bubble flow, the vortical-spiral flow, and the turbulent flow. The vortical-spiral flow was regarded as an unstable transition regime between the dispersed bubble and the turbulent flow regimes, and can be grouped into four local subregions, i.e., descending flow, vortical-spiral flow, fast bubble flow, and central plume. From the experimental curves of gas holdup vs gas velocity, Zahradnik and Fialova[7] and Zahradnik et al.[6] found that the transition regime began to occur at 0.04 m/s of gas velocity, and the flow reached the fully developed turbulent regime for U_g greater than 0.12 m/s. In the latter case, the hydrodynamics of columns is mainly determined by the bulk liquid circulation and the primary gas dispersion plays minor role.[7] Ruzicka et al. [25] distinguished the heterogeneous regimes into THeR (heterogeneous regime resulting from the instability of homogeneous regime and its subsequent transition at high gas velocities) and PHeR (pure heterogeneous regime spanning the whole range of gas velocities). As reported by Ruzicka et al.,[25] THeR occurs when using small and closely spaced orifices, whereas PHeR occurs when using large orifices. With increasing gas flow rate, the gas holdup curves of these two cases first split at low and medium gas velocities and then rejoin again at high gas velocities when the transition to THeR is completed.

Various models have been developed to predict the regime transition in gas−liquid flow, such as the drift flux models[26,27] summarized by Ruzicka et al.[25] as well as the linear stability theory.[28,29] It is found that the formulation of the added mass force[30] and the lift force[31] are critical for linear stability theories. Computational fluid dynamics (CFD) has emerged as a powerful tool for simulating the hydrodynamics of gas−liquid flow in recent years. In parallel with its quick development and application in process industries, there is still much uncertainty to be resolved, such as the modeling of turbulence and of bubble breakup and coalescence. Monahan[32] investigated the influence of various formulation of two-fluid models on the simulation of flow regime transition, and found that the ability of CFD models depends greatly on force models, turbulence models and grid resolution.

Despite these efforts, the nature of regime transition is still far from being well understood. For investigating the compli-

* To whom correspondence should be addressed: Tel: 86-10-82627076. Fax: 86-10-62558065. E-mail: nyang@home.ipe.ac.cn.

† State Key Laboratory of Multi-Phase Complex Systems, Institute of Process Engineering, Chinese Academy of Sciences.

‡ Graduate School of Chinese Academy of Sciences.

10.1021/ie8003623 CCC: $40.75
Published on Web 08/05/2008

cated multiscale structure in gas−solid systems, the so-called energy-minimization multiscale (EMMS) model was proposed by Li et al.[33] and Li and Kwauk[34] through the establishment of a stability condition. This has been accomplished by analyzing the compromise between two dominant mechanisms in fluidized beds, namely, the tendency for the fluid to pass through the particle layer with least resistance featured by the minimization of the volume-specific energy consumption for suspending and transporting particles W_{st}, and the tendency for the particles to maintain least gravitational potential reflected by the minimization of the local average voidage ϵ. The stability condition was formulated as $N_{st} = W_{st}/\rho_p(1-\epsilon) = \min$ (N_{st} denotes the mass-specific energy consumption for suspending and transporting particles) which reflects the compromise between these two tendencies. The EMMS model has been successfully employed to predict the choking phenomena, viz., the regime transition between dilute transport and fast fluidization.[35,36] This strategy was further generalized into the so-called analytical multiscale method and thus efforts were also made to seek the stability conditions for other complex systems including turbulent flow, foam drainage, granular flow, nano-gas−liquid flow, and emulsion systems.[37]

Zhao[38] and Ge et al.[37] tried to extend the principles of the analytical multiscale method to gas−liquid bubbly flow by resolving the energy consumption and proposing tentatively a stability condition for the system. Recently, Yang et al.[39] established a dual-bubble-size (DBS) model based on these works. For air/water systems, the calculation of this DBS model indicated a jump change of gas hold-up at a critical gas velocity. It was attributed to the jump change of the global minimum point between two local minima of energy dissipated directly through microscopic interactions of gas and liquid. Then these jump changes were used to explain the physical nature of the transition from the homogeneous to the fully developed heterogeneous regime. The objective of this study is to further clarify the occurrence and variation of the jump change in 3D space of structure parameters, and explore some remaining issues in the DBS model such as the influence of drag coefficient correlations. Furthermore, the DBS model is employed to predict the regime transition for aqueous saccharose and glycerin solution systems with consideration to the influence of liquid viscosity and surface tension. Finally, the dominant mechanisms for various regimes and the relationship between the compromise of dominant mechanisms with bubble dynamics are analyzed in an attempt to generally explore the stability condition for gas−liquid systems.

2. Reiteration of the DBS Model

The DBS model proposed by Yang et al.[39] resolves the heterogeneous structure of gas−liquid flow into two bubble classes according to the bimodal bubble size distribution found in experiments.[9,40–42] The small and large bubble classes are characterized respectively by their equivalent bubble diameters (d_S and d_L), its corresponding volume fractions (f_S and f_L) and superficial gas velocities ($U_{g,S}$ and $U_{g,L}$). The liquid flow field is not resolved on the assumption that the two bubble classes share the same liquid flow field and the bubbles breakup under the common circumstances of turbulent flow. The conservation equations are formulated in Table 1.

Neglecting boundary effects, the mechanical energy is considered to consume on two scales: on the microscale, the energy is transferred from gas to liquid due to the relative motion between bubbles and liquid. One part of the energy is then dissipated through liquid turbulence. The other leads to the deformation and oscillation of bubble surfaces and finally dissipates on microscale. The energy consumptions with respect to unit mass of liquid for the above two portions were denoted as N_{turb} and N_{surf}, respectively, both of which compose the energy dissipation directly through microscopic interactions. Of course, these energy dissipation terms may have a delicate relationship with the complicated flow structures in the liquid phase, like the shear-induced or bubble-induced turbulence, as well as the bubble wakes reported in literature and, therefore, needs further investigation.

However, energy may also be transferred from the bulk of liquid to the surface of daughter bubbles due to bubble breakage and then dissipate during the coalescence of bubbles. This portion of energy is thought to occur on meso-scale and is denoted as N_{break} for unit mass of liquid. The term "meso-scale" can be understood from the perspective that bubbles typically break up at one location and coalesce at another, spanning a relatively "longer" spatial and temporal distance as compared with the viscous dissipation in liquid, N_{turb}, and the dissipation on bubble surface, N_{surf}. Whether there exists other more reasonable ways for scale differentiation is still an open question.

Table 1. Conservation Equations of the DBS Model[a]

continuity equation:

$$\sum_i U_{g,i} = U_g \tag{1}$$

force balance equations:

$$f_i\rho_l g = \frac{f_i}{\pi/6 \cdot d_i^3} \cdot C_{Di}\frac{\pi}{4}d_i^2 \cdot \frac{1}{2}\rho_l\left(\frac{U_{g,i}}{f_i} - \frac{U_l}{1-f_b}\right)^2 \tag{2}$$

constitutive correlations:

$$C_{D,i} = C_{D0,i}(1-f_b)^4 \tag{3}$$

$$C_{D0,b} = \frac{4}{3}\frac{g d_b}{U_T^2}\frac{\rho_l - \rho_g}{\rho_l} \tag{4}$$

$$U_T = \frac{\mu_l}{\rho_l d_b}M^{-0.149}(J - 0.857) \tag{5}$$

where

$$M = \frac{\mu_l^4 g(\rho_l - \rho_g)}{\rho_l^2 \sigma^3} \tag{6}$$

$$J = \begin{cases} 0.94H^{0.757} & (2 < H \le 59.3) \\ 3.42H^{0.441} & (H > 59.3) \end{cases} \tag{7}$$

$$H = \frac{4}{3}Eo \cdot M^{-0.149}\left(\frac{\mu_l}{\mu_{ref}}\right)^{-0.14} \tag{8}$$

and

$$Eo = \frac{g(\rho_l - \rho_g)d_b^2}{\sigma} \tag{9}$$

[a] The index "i" represents "S" and "L" for small bubble phase and large bubble phase respectively.

Table 2. Energy Resolution and the Stability Condition for the SBS/DBS Model[a]

energy resolution:

SBS model:
$$(N_{surf} + N_{turb}) + N_{break} = gU_g \tag{10}$$

DBS model:
$$\sum_i N_{surf,i} + N_{turb} + \sum_i N_{break,i} = gU_g \tag{11}$$

constitutive correlations:
$$N_{surf,i} = U_{g,i}g\frac{C_{D,bi} - C_{D,pi}}{C_{D,bi}} = U_{g,i}g\frac{C_{D0,bi}(1-f_b)^4 - C_{D0,pi}(1-f_b)^4}{C_{D0,bi}(1-f_b)^4} \tag{12}$$

where
$$\begin{cases} C_{D0,p} = \dfrac{24}{Re}(1 + 0.15Re^{0.687}) & (Re < 1000) \\ C_{D0,p} = 0.44 & (Re > 1000) \end{cases} \tag{13}$$

$$N_{break,i} = \int_{\lambda_{min}}^{d_i}\int_0^{0.5} \frac{\omega(d_i, f_i, \lambda)}{(1-f_b)\rho_l + f_b\rho_g} \cdot P_b(d_i, \lambda, f_{BV}) \cdot c_f\pi d_i^2\sigma \cdot df_{BV}d\lambda \tag{14}$$

where
$$\omega(d_i, f_i, \lambda) = 0.923(1-f_i)n_i N_{turb}^{1/3}\frac{(\lambda + d_i)^2}{\lambda^{11/3}} \tag{15}$$

$$P_b(d_i, \lambda, f_{BV}) = \exp\left[-\frac{\max\{c_f\pi d_i^2\sigma, \pi\sigma\lambda^3/(3d_i f_{BV}^{1/3})\}}{\rho_l \cdot (\pi/6)\lambda^3 \cdot (\lambda N_{turb})^{2/3}}\right] \tag{16}$$

Stability condition:

SBS model:
$$N_{surf} + N_{turb} = \min \tag{17}$$

DBS model:
$$\sum_i N_{surf,i} + N_{turb} = \min \tag{18}$$

[a] The index "i" represents "S" and "L" for small bubble phase and large bubble phase respectively.

On the basis of these considerations, Zhao[38] and Ge et al.[37] proposed that lower N_{turb} indicates weaker local fluctuation in liquid phase and hence larger bubbles, whereas lower N_{surf} indicates weaker surface oscillation and hence smaller and spherical bubbles. Investigating the compromise of these two dominating mechanisms leads to the formulation of the stability condition for the overall behavior, namely, the minimization of energy dissipation directly through microscopic interactions ($N_{surf} + N_{turb} = \min$). This stability condition was employed to close their single-bubble-size (SBS) model.

Yang et al.[39] extended the way of energy resolution and the stability condition into the dual-bubble-size (DBS) model, and therefore the small and large bubbles hold their respective energy dissipation terms for bubble breakage and bubble oscillation, namely, $N_{break,S}$, $N_{break,L}$, $N_{surf,S}$, and $N_{surf,L}$. The energy dissipation, N_{turb}, is not resolved on the assumption that the two bubble classes share the same liquid flow field. The formulation of different energy dissipation terms and stability condition is listed in Table 2.

The model is composed of six variables (d_S, d_L, f_S, f_L, $U_{g,S}$, and $U_{g,L}$), three conservation equations, and a stability condition. The variables d_S, d_L, and $U_{g,S}$ were selected as the open variables constructing the three-dimensional space of structure parameters. Then the nonlinear optimization problem was solved by an ergodic global algorithm to search the global minimum of the energy dissipation directly on microscale ($N_{surf} + N_{turb}$) among all valid combinations of the three open variables. The calculation of Yang et al.[39] indicated that the landscape of ($N_{surf} + N_{turb}$) is rather complicated in the parameter space, exhibiting multiple local minima and strong dependence on the drag correlations.

Figure 1 illustrates the comparison among the prediction from the DBS and SBS models, the experiments of Camarasa et al.,[9] and three empirical correlations for air–water systems. One distinct feature of this calculation is the jump change of gas hold-up between 0.128m/s and 0.129m/s, as illustrated by the dashed line of Figure 1. This was considered to correspond to the experimental findings of Zahradnik et al.[7] and Camarasa et al.[9] that the fully developed heterogeneous regime was observed for gas velocity beyond 0.125 m/s. The reason for this jump change can be illustrated by the contour plots of energy directly dissipated on microscales shown in Figure 2. For U_g less than

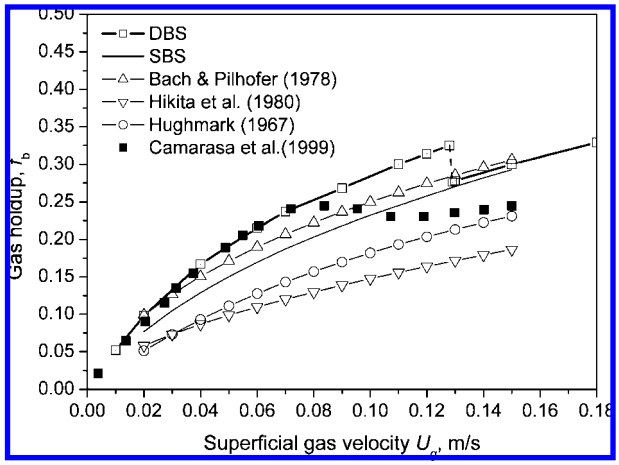

Figure 1. Comparison among model prediction, experiments, and empirical correlations for gas hold-up (Yang et al.[39]).

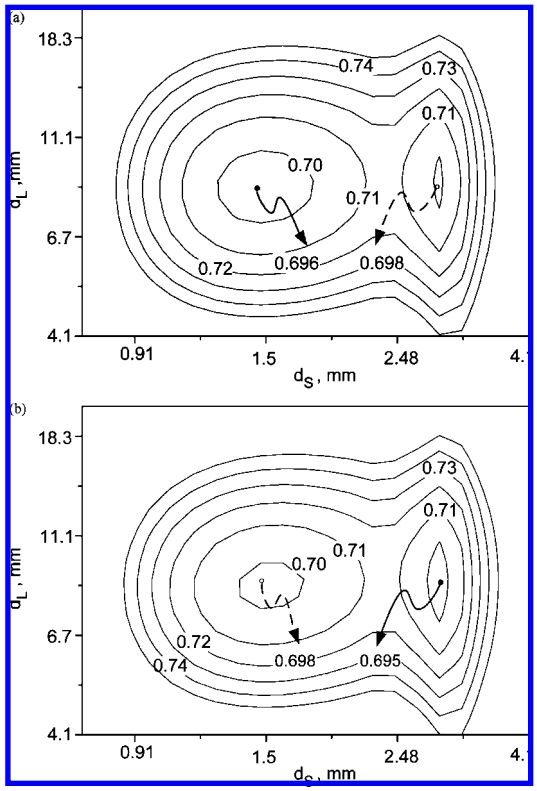

Figure 2. Shift of the global minimum point between the two valleys: the contour plot of $(N_{surf} + N_{turb})/N_T$ in the 2D space of structure parameters (d_S, d_L): (a) $U_g = 0.128$ m/s, $U_{g,S} = 0.0845$ m/s; (b) $U_g = 0.129$ m/s, $U_{g,S} = 0.0916$ m/s (adapted from Yang et al.[39]).

or equal to 0.128m/s, the global minimum lies in the left valley of the contour plot, whereas it shifts to the right valley for U_g equal to or greater than 0.129m/s. This shift on the contour plot gives rise to the jump change of structural parameters and therefore could provide a physical explanation on the regime transition to fully developed heterogeneous regime.

It should be noted that the variation of gas hold-up is also subject to the influence of column sizes and sparger types. Since these factors are not considered in the current DBS model, it is difficult to expect close consistency between experimental data and the model calculation. This conceptual model at present is only expected to qualitatively reflect the general trend of structural variation and regime transition and offer some physical explanation for these phenomena. Also, the lift and added mass forces, which were reported to play important role in flow pattern,[23,31,43] are not considered in current DBS model for simplicity.

3. Jump Change of the Model Calculation

Although the jump change was captured by inspecting the two contour plots shown in Figure 2, the continuous variation of the global minima with gas velocities in the three-dimensional parameter space was not detailed in our previous work. To understand the occurrence of the jump change and reveal the underlying mechanisms, the shape of iso-surface of $(N_{surf} + N_{turb})/N_T$ and the slice where the global minimum point is located for different velocities is shown in Figure 3.

Note that each point in the parameter space (d_S, d_L, U_{gS}) can find its image if it is reflected first with respect to the plane of $U_{g,S} = 0.5U_g$ and then the diagonal plane of $d_S = d_L$. For this reason, only the subspace ($d_S < d_L$) at the right of the symmetrical plane of $d_S = d_L$ is relevant in our discussion, and hence the subscripts "S" and "L" in the subsequent parts of this work represent the practical small and large bubble classes, respectively.

For lower gas velocities, only one local minimum viz. the global minimum is found (Figure 3, parts a and b). Whereas two local minima appear for U_g beyond some critical value as shown in Figure 3c, and correspondingly, two connective ellipsoids of the iso-surface can be observed. With the further increase of U_g, the location of global minimum jumps from the right ellipsoid (Figure 3d) to the left one (Figure 3, parts e and f).

To show the variation tendency of structural parameters, the trajectory of the global minimum point with the increase of superficial gas velocities is traced out in Figure 4. Clearly observable is the initial continuous rise of the global minimum points with increasing gas velocity and the subsequent jump change between 0.128 and 0.129 m/s of gas velocities, as illustrated by the dash line of Figure 4. Then the continuous rise appears over again for U_g greater than 0.129 m/s. With the increase of U_g, the large bubble diameter d_L decreases and small bubble diameter d_S increases gradually when $U_g < 0.128$ m/s. Then the small bubble diameter jumps from about 1.4 mm to 2.9 mm when U_g varies from 0.128 to 0.129 m/s. It can be concluded that this jump change drives the evolution and the abrupt change of structural parameters and therefore leads to regime transition. As reported in our previous work,[39] the abrupt increase of the small bubble diameter is also accompanied by the dramatic decrease of total and small bubble gas hold-up as well as the rise of relative frequency of large bubble, suggesting that the system reaches the state of fully developed heterogeneous regime.

4. Influence of the Drag Coefficient

Drag correlations listed in Table 3 are adopted to investigate the influence of drag coefficients on the calculation of DBS model. It is reported that Grace's correlation[44] is suitable for pure liquids over wide range of properties and deviation is visible for spherical, cap-shaped bubbles.[45] For air−water systems, the minimum bubble diameter for using this correlation is restricted to 0.55 mm ($H > 2$, see eq), and hence limits the searching range of domain in the DBS model. Considering the similarity between the bubble interfacial disturbances and waves in ideal fluid, Mendelson[46] proposed a terminal velocity correlation suitable for pure liquids in the inviscid flow regime which was subdivided into surface tension- and buoyancy-

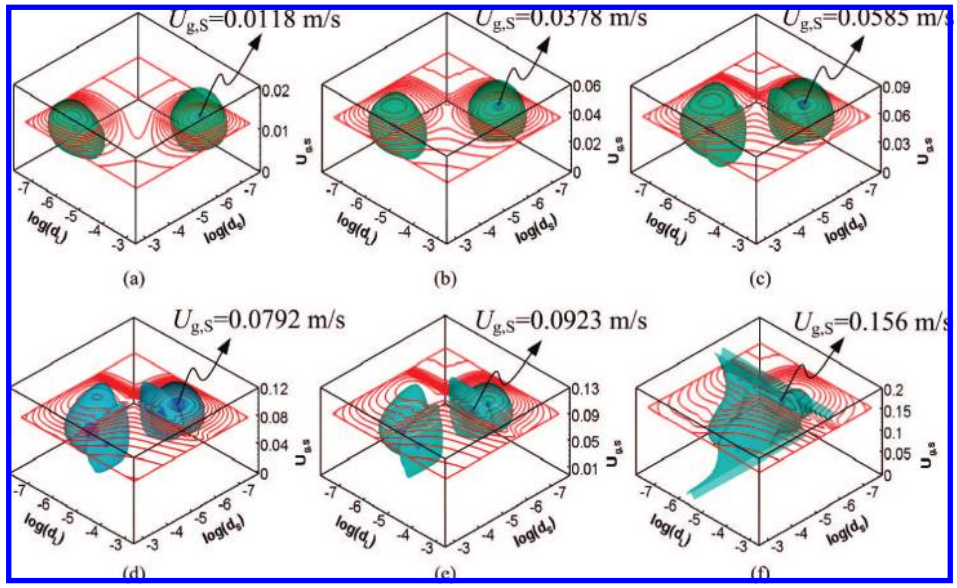

Figure 3. The iso-surface of $(N_{surf} + N_{turb})/N_T$ and the $U_{g,S}$-plane where the global minimum point is located in the 3D space of structure parameters (d_S, d_L, $U_{g,S}$). Natural logarithm scales are used for d_S and d_L with dimensions of meters. (a) $U_g = 0.02$ m/s; (b) $U_g = 0.06$ m/s; (c) $U_g = 0.09$ m/s; (d) $U_g = 0.12$ m/s; (e) $U_g = 0.13$ m/s; and (f) $U_g = 0.20$ m/s.

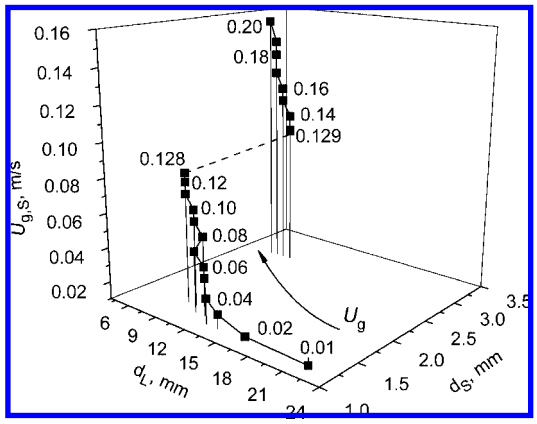

Figure 4. Trajectory of the point with global minimum of $(N_{surf} + N_{turb})/N_T$ in the 3D parameter space with increasing U_g.

dominant regimes. To acquire a continuous correlation for the viscous regime and the surface tension-dominant regimes, Fan and Tsuchiya[47] developed a general correlation of bubble terminal velocity which is applicable for both pure and contaminated systems. In correlation 20 of Table 3, V_{T1} and V_{T2} denote terminal velocity in the viscous regime and the distorted/cap bubble (surface tension-dominant) regime respectively. This correlation improves Mendelson's model[46] in two aspects: the viscous effect is considered by adding the term of V_{T1} and the liquid physicochemical properties by the coefficients c and n. The three aforementioned drag coefficient models are independent of slip velocity and C_{D0} can be obtained from eq (4) of Table 3, whereas Tomiyama's correlations[43] give C_{D0} directly.

Figure 5 indicates that the drag coefficients reach their minimum at about 3 mm for Grace's correlation and 1.4 mm for Fan's correlation. Mendelson's correlation gives a monotonous increase until a maximum with increasing bubble diameter. At the small bubble region, Tomiyama's correlation is dependent upon the slip velocities and the drag coefficient is close to the calculation of Fan's model. At large bubble region, the curve of Tomiyama's correlation coincides with that of Mendelson's correlations, whereas Grace's correlation shows a rapid increase for $d_b > 10$ mm.

Figure 6 shows the shape of iso-surface of $(N_{surf} + N_{turb})/N_T$ for different drag correlations. Since no constraint on the minimum bubble diameter d_{min} is reported for the correlations listed in Table 3 except for Grace's correlation, we extend the searching range of bubble size to 0.01 mm for Mendelson's and Tomiyama's correlations. For Mendelson's correlation, the global minimum of $(N_{surf} + N_{turb})/N_T$ always locates at the vertical boundary plane of d_{min} assumed. However, it has been reported that this drag correlation is only suitable for bubble diameters greater than 2 mm in pure liquids and needs modification for very small bubble and contaminated liquids.[45] On the contrary, the global minimum locates in the interior of the parameter space when other correlations are used, and thus the calculation of the DBS model is irrelevant to the d_{min} assumed.

Since Grace's correlation deviates from other correlations for large bubble region, we correct this correlation by employing Mendelson's correlation when H defined in eq 8 is greater than 59.3. It can be seen from Figure 7 that the calculation with the combined model of Grace and Mendelson is very close to that with Grace's correlation alone. Both curves indicate jump change of the total gas hold-up. This implies that the deviation of drag coefficient in large bubble region shown in Figure 5 plays minor role in the model prediction of regime transition. While Tomiyama's correlation shows a completely different characteristic in that the gas hold-up increases monotonously with increasing superficial gas velocity. Fan's correlation acts in a way similar to Tomiyama's correlation, but a thorough inspection shows that there is still a slight jump between 0.12 and 0.121 m/s.

The difference of gas hold-up curves can be explained by the difference of trajectories shown in Figure 8. No jump change is observed in the curve of Tomiyama's correlation and the small bubble diameter is always around 2.4 mm, whereas the other two correlations produce jump change. Compared with the dramatic jump change of Grace's correlation, the curve of Fan's correlation indicates a relatively smaller jump change of the small diameter from 1.8 mm at $U_g = 0.12$ m/s to 2.4 mm at U_g

Table 3. Correlations for Different Drag Coefficient Models

investigator	correlation		usable condition
Grace:[44]	>eqs 5–9		pure liquids over wide properties; Eo < 40; M < 10−3; Re > 0.2
Mendelson:[46]	$V_T = \sqrt{\frac{2\sigma}{d\rho} + \frac{gd}{2}}$	(19)	pure liquids; d > 2 mm
Fan and Tsuchiya:[47]	$V_T = (V_{T1}^{-n} + V_{T2}^{-n})^{-1/n}$	(20)	pure liquids: K_{b0} = 14.7; n = 1.6; c = 1.2; contaminated systems: K_{b0} = 10.2; n = 0.8; c = 1.4
	where		
	$V_{T1} = \frac{\rho_l g d^2}{K_b \mu_l} V_{T2} = \sqrt{\frac{2c\sigma}{d\rho l} + \frac{gd}{2}}$	(21)	K_{b0} = 10.2; n = 0.8; c = 1.4; no limits in size
	$K_b = \max(12, K_{b0} Mo^{-0.038}) Mo = \frac{\Delta\rho g \mu_l^4}{\sigma^3 \rho_l^2}$	(22)	
Tomiyama:[43]	$C_{D0,b} = \max\left[\min\left[\frac{16}{Re}(1 + 0.15Re^{0.687}), \frac{48}{Re}\right], \frac{8}{3}\frac{\mathbf{Eo}}{\mathbf{Eo}+4}\right]$	(23)	pure water
	$C_{D0,b} = \max\left[\min\left[\frac{24}{Re}(1 + 0.15Re^{0.687}), \frac{72}{Re}\right], \frac{8}{3}\frac{Eo}{Eo+4}\right]$	(24)	slightly contaminated
	$C_{D0,b} = \max\left[\frac{24}{Re}(1 + 0.15Re^{0.687}), \frac{8}{3}\frac{Eo}{Eo+4}\right]$	(25)	contaminated

= 0.121 m/s. This difference of trajectories can be used to explain the gas hold-up curves shown in Figure 7.

These differences in trajectory and hence the variation of gas hold-up can attribute to the calculation of energy dissipation, N_{surf}, for small bubbles. According to eq 12, N_{surf} approaches zero if Tomiyama's or Fan's correlations are employed due to the fact that these correlations make little difference between the drag coefficient of bubbles and particles for small bubbles.

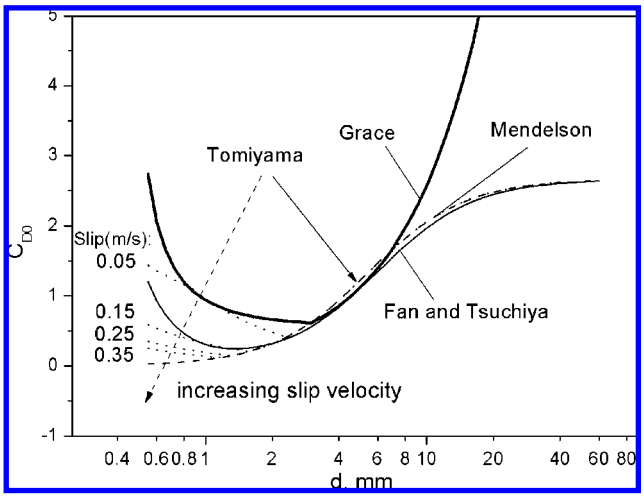

Figure 5. Comparison of different drag coefficient correlations. Note that the curves of Tomiyama coincide with that of Mendelson for larger bubbles, but is dependent on slip velocity for smaller bubbles, as denoted by the broken lines.

Alternatively, by using Grace's correlation for small bubble region, the DBS model does generate a certain amount of energy dissipation for bubble oscillation. Clift et al.[48] claimed that the onset of bubble oscillation is about Re = 450 and therefore N_{surf} should be a nonzero value for small bubbles within 1.4 mm and 3 mm. The problem is essentially related to the model for calculating N_{surf}, suggesting that more appropriate model for calculating N_{surf} needs to be established. In fact, the combined model of Fan's or Tomiyama's model for large bubble region with Grace's model for small bubble region can also capture the jump change, since these two models are very close to Mendelson's model at large bubble region, as indicated in Figure 5 and Figure 7.

It is interesting to see that even using Grace's correlation the calculation of gas hold-up from the single-bubble-size (SBS) model does not indicate any jump change as shown in Figure 7. Rather, it is almost consistent with the DBS model calculation using Tomiyama's or Fan's correlations. The main difference between the SBS model and the DBS model is that the heterogeneous structure characterized by two bubble classes is considered in the latter, which may give rise to the jump change. Similarly, the ability of reflecting the structural heterogeneity in the DBS model may be lost if N_{surf} for small bubbles could not be identified. It is this ability of the model to describe the structural heterogeneity which leads to the calculation of the jump change.

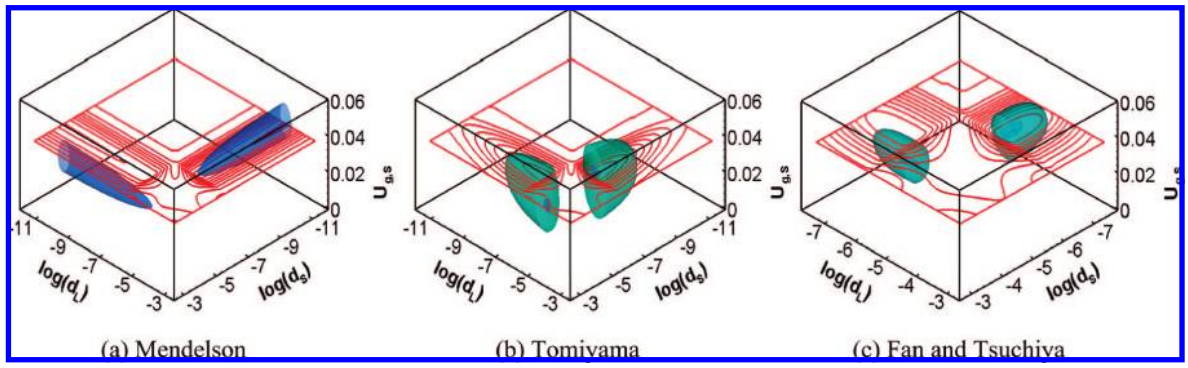

Figure 6. The iso-surface of $(N_{surf} + N_{turb})/N_T$ for different drag correlations at $U_g = 0.06$ m/s.

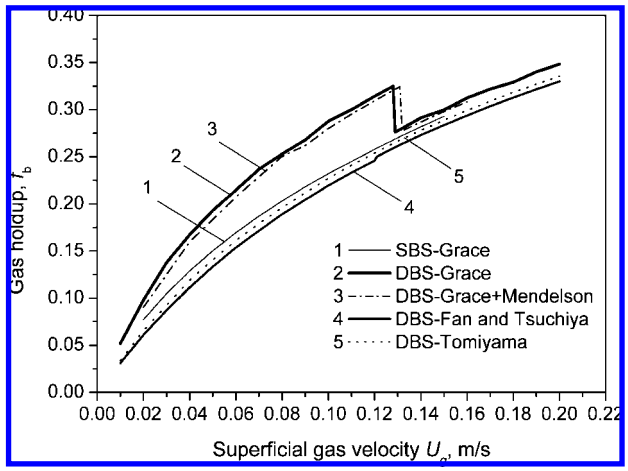

Figure 7. Calculated gas hold-up using different drag coefficient correlations.

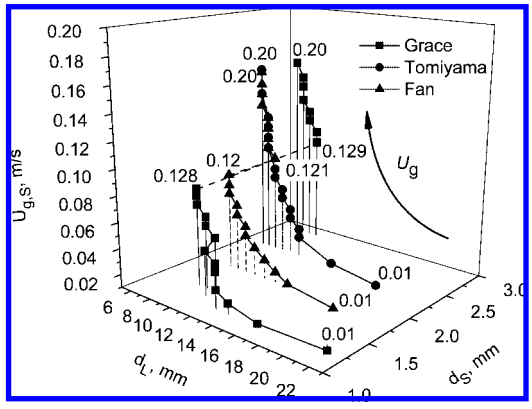

Figure 8. Trajectories of the global minimum points of $(N_{surf} + N_{turb})/N_T$ for different drag correlations.

5. Effect of Liquid Viscosity

Liquid viscosity is reported to have significant effects on the flow behavior of bubble columns.[49–51] Zahradnik et al.[6] found that when viscosity exceeds some critical value (8 mPa·s), the flow will always be in the state of heterogeneous regime for the whole range of gas velocity, even for the distributing plate which typically generates homogeneous bubbling regime at lower velocity in low viscous fluids. This can be illustrated in Figure 9 that for the cases of A2 and A3 with higher viscosities, the experimental curves show monotonic increase; whereas for the cases of pure water and A1 with lower viscosities, the experimental curves exhibit maxima or plateau-like forms. The DBS model calculation shows that the curve of A2 deviates

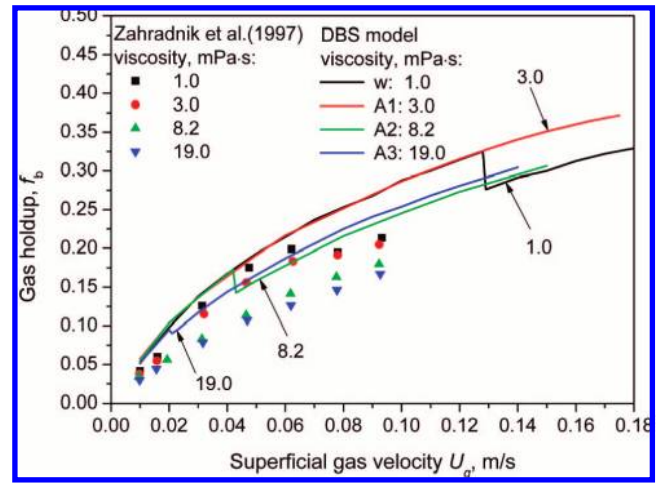

Figure 9. Comparison between the experiment of Zahradnik et al.[6] and the DBS calculation for saccharose solution: effect of viscosity on regime transition. w: pure water ($\rho_l = 998$ kg/m^3; $\mu_l = 1.0$ mPa·s; $\sigma = 72$ mN/m); A1: 30wt% ($\rho_l = 1125$ kg/m^3;$\mu_l = 3.0$ mPa·s; $\sigma = 73.87$ mN/m); A2: 43wt% ($\rho_l = 1189$ kg/m^3;$\mu_l = 8.2$ mPa·s; $\sigma = 73.9$ mN/m); A3: 52wt% ($\rho_l = 1238$ kg/m^3;$\mu_l = 19.0$ mPa·s; $\sigma = 73.91$ mN/m).

from the pure water case at about 0.043 m/s and the deviation of A3 curve occurs more earlier (0.021 m/s). The advance of jump change implies that the homogeneous regime is suppressed at higher viscosity ($\mu_l > 8.0$ mPa·s), which is in reasonable agreement with experimental results. However, Ruzicka et al.[52] reported that the slight increase in liquid viscosity (1−3 mPa·s) could stabilize the homogeneous regime. This finding can also be supported by our calculation of case A1: jump change could not be observed for U_g less than 0.17 m/s, which implies that the transition to fully developed heterogeneous regime may vanish or at least be deferred to higher gas velocity compared with the pure water case.

Similar trends can also be reflected in Figure 10 for aqueous glycerin systems. The deferment of the jump change in the curve of B1 at higher gas velocities indicates that a slight increase of viscosity can stabilize the homogeneous flow. The advance of the jump change in the curve of B2 at lower gas velocities indicates unfavorable effects of liquid viscosity on the stability of the homogeneous regime. Furthermore, the jump change in the curves of B3 and B4 at much higher viscosities is so small and even inconspicuous that it may indicate some weak transition, meaning we are left with no means to experimentally ascertain it.

The advance of jump change for gas holdup is accompanied by the difference in the variation trend of structure parameters between the cases of pure water and liquid with higher

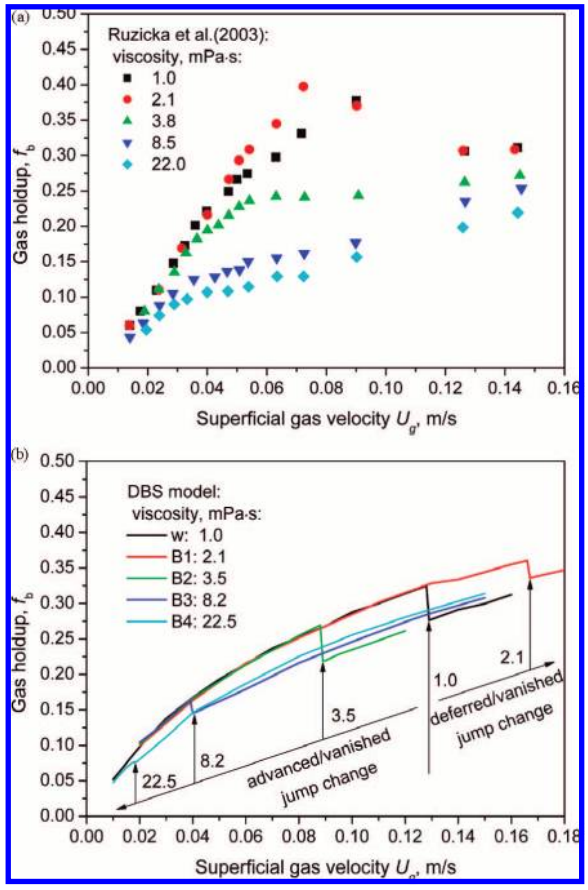

Figure 10. Comparison between the experiment of Ruzicka et al.[52] and the DBS calculation for glycerin solution: effect of viscosity on regime transition. (a) adapted from Ruzicka et al.;[52] (b) calculation by the DBS model. B1: $\rho_l = 1020$ kg/m^3; $\mu_l = 2.1$ mPa·s; $\sigma = 72$ mN/m; B2: $\rho_l = 1081$ kg/m^3; $\mu_l = 3.5$ mPa·s; $\sigma = 70$ mN/m; B3: $\rho_l = 1126$ kg/m^3; $\mu_l = 8.2$ mPa·s; $\sigma = 68$ mN/m; B4: $\rho_l = 1173$ kg/m^3; $\mu_l = 22.5$ mPa·s; $\sigma = 67$ mN/m.

viscosity. Figure 11a shows that large and small bubbles exchange their variation trend of gas hold-up at the jump change point and therefore the system varies from "small bubble-rich" state to "large bubble-rich" state for the higher viscosity case. Whereas the small bubble gas hold-up is always greater than that of large bubble for pure water and the lower viscosity case (A1), as shown in Figure 11, parts b and c. Figure 12a shows that compared to the abrupt rise of small bubble diameter when jump change occurs in pure water systems, the large bubble diameter exhibits a dramatic decrease for higher viscosity case. It can be seen from Figure 12b that the jump change reflected by the abrupt increase of small bubble size for pure water is deferred or disappears for case A1. This may attribute to the stabilizing effect of liquid viscosity on small bubble phase by suppressing the bubble oscillation or bubble coalescence.

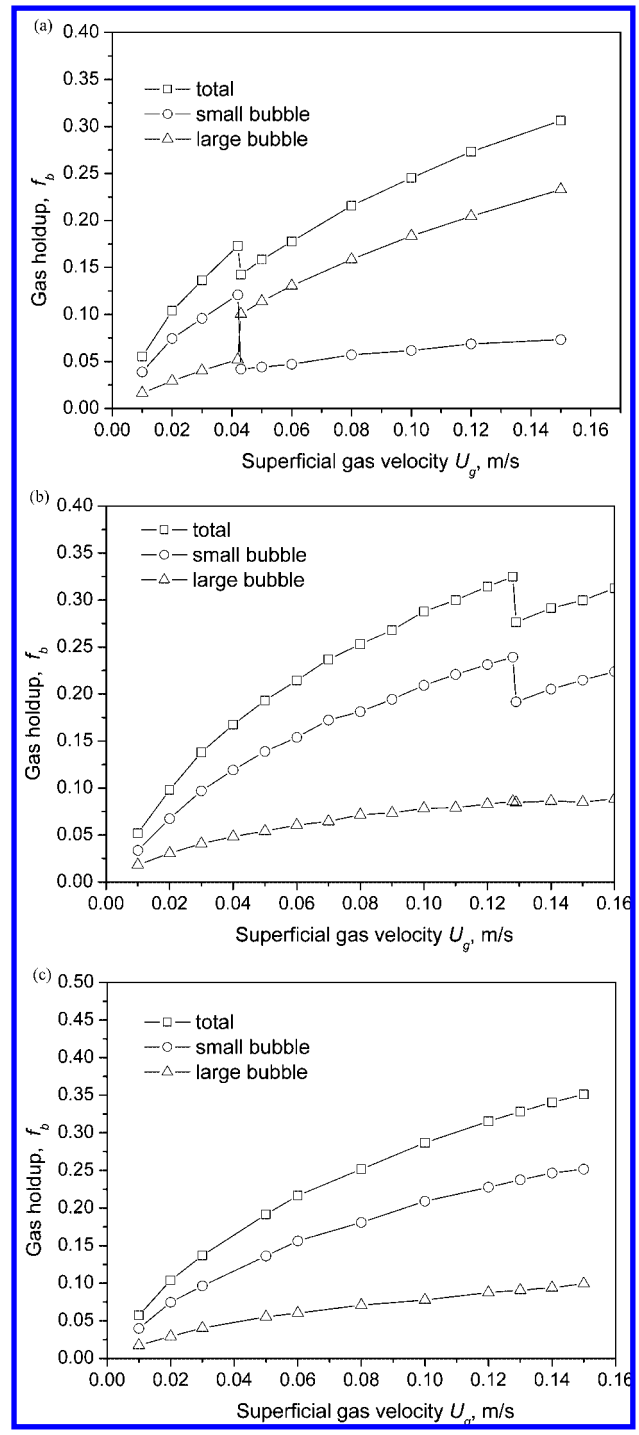

Figure 11. Variation of the holdup of small and large bubbles with superficial gas velocity: (a) 43wt% saccharose solution ($\mu_l = 8.2$ mPa·s), (b) pure water ($\mu_l = 1.0$ mPa·s), and (c) 30wt% saccharose solution ($\mu_l = 3.0$ mPa·s.

6. Prospects: Compromise between Dominant Mechanisms

The key step of the so-called analytical multiscale method in exploring the complexity of multiscale spatio-temporal structures is to analyze the compromise between dominant mechanisms and hence establish the stability condition reflecting correlations between different scales.[37,53] The dominant mechanisms can be formulated as extremum tendencies, and their compromise can be expressed as a mutually constrained extremum. The stability condition reflecting this mechanism of compromise is adopted to close the incomplete conservation equations. This method can date back to the original work of the energy-minimization multiscale (EMMS) model for gas−solid flow.[33,34] Following this clue, we attempt to analyze the dominant mechanisms on different scales to explore the complexity of gas−liquid systems.

6.1. Understanding Compromise from the DBS Model Calculation. As mentioned earlier, the stability condition in the DBS model is formulated as $N_{surf} + N_{turb} = \min$ to reflect the compromise between two dominant mechanisms, namely, $N_{surf} = \min$ and $N_{turb} = \min$. In turn, the calculation of the DBS

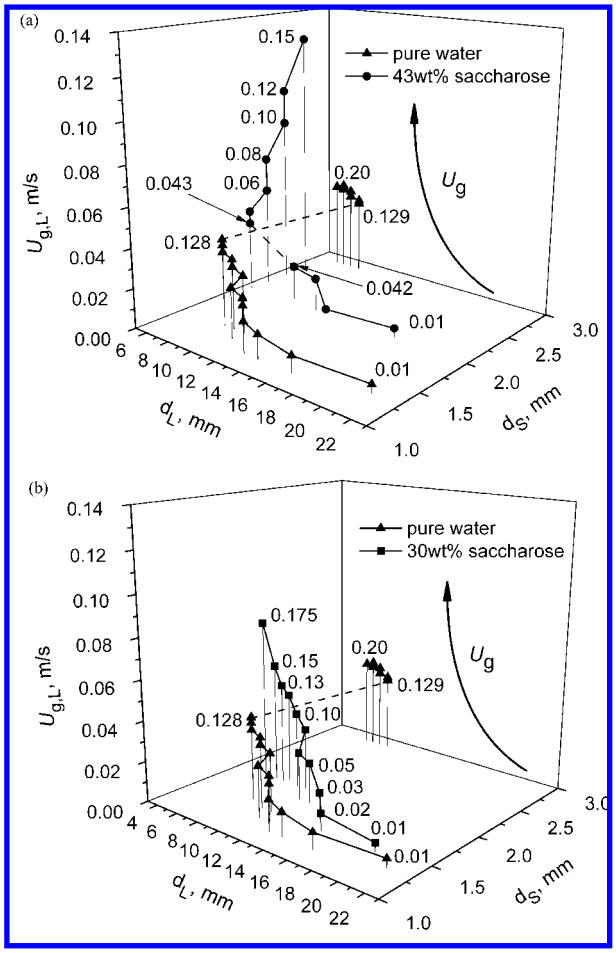

Figure 12. Trajectories of the global minimum points of $(N_{surf} + N_{turb})/N_T$ for cases of different liquid viscosity compared with pure water: (a) aqueous solution of 43 wt% saccharose (μ_l = 8.2 mPa·s) and (b) aqueous solution of 30 wt% saccharose (μ_l = 3.0 mPa·s).

model can also supply some comprehension on the two dominant mechanisms.

Figure 13 shows the 3-D contour plots for N_{surf}/N_T, N_{turb}/N_T, and $(N_{surf} + N_{turb})/N_T$ for U_g = 0.06 m/s. Apparently, N_{surf}/N_T attains a minimum only when both classes of bubbles are equal and small (see the inner corner of the cube), whereas the minimum of N_{turb}/N_T lies at the outer corner of the cube which indicates that both classes of bubbles are equal and large. However, the minimum point for the sum of these two energy dissipation terms, i.e., $(N_{surf} + N_{turb})/N_T$, falls within the ellipsoid, which indicates the coexistence of small and large bubbles in the system. This implies that the joint effect or the compromise of these two mechanisms leads to the heterogeneous bubble-size distribution.

6.2. Dominant Mechanisms for the Behavior of a Single Bubble. Bubble dynamics such as bubble formation, bubble shape, and bubble rise velocity, as well as bubble-induced liquid flow have raised much attention in the literature.[45,47,48,54] Mendelson[46] and Fan[47] proposed drag coefficient correlations on the basis of the analysis of the dominant mechanisms for a single bubble, and the dominant factors of the system were considered to be viscosity, surface tension, and buoyancy with increasing bubble diameter, as shown in Figure 14.

The dominant mechanisms may also be understood from another perspective as a way of analyzing gas−solid flow in the energy-minimization multiscale (EMMS) model proposed by Li et al.[33] and Li and Kwauk.[34] When the bubble is very small, the viscous effect is dominant and the liquid takes over dominance of the bubble behavior. The bubble is constrained by surrounding the liquid and hence acts in the similar way as rigid solid particles. In another ultimate case of the very large bubble, the shape will be almost fixed like a spherical cap and rise in a rectilinear way. The flow in this case is gas-dominated, and the local flow field is dictated by the movement of the large bubble. However, moderate bubbles are reported to take on rather complicated shapes and behaviors. The shape may be ellipsoidal, dimpled, skirted, or wobbling,[48] and the trace may be zigzag or spiral.[55] These complicated behaviors could be envisioned to be related to the compromise between liquid-dominant and gas-dominant mechanisms from a microscale viewpoint. The turning of the drag coefficient curve for the moderate bubble may indicate the switch between the two dominant mechanisms.

6.3. Dynamics of Compromise: Bubble Coalescence and Breakup. In bubble columns, the properties of bubbles are generally unstable and subject to the influence of liquid turbulence, interfacial instability, wake entrainment, size dependent rise velocity difference, and shear layer-induced velocity difference. Recent years have witnessed the rapid development of population balance model (PBM) which has been combined with computational fluid dynamics (CFD) to predict the variation of bubble sizes and flow behavior.[56,57] The average bubble size for each local cell can be obtained from the solution of population balance equations. In the DBS model, the equivalent bubble size is believed to be the result of compromise between two dominant mechanisms, i.e., N_{surf} = min and N_{turb} = min.

A rational explanation on the relationship between the concept of compromise used in the DBS model and the bubble coalescence and breakup described by PBM can be illustrated in Figure 15. If a large bubble is bombarded by eddies with sufficient kinetic energy, then it would break into two or more daughter bubbles. When this event happens, the energy which is dissipated for bubble surface oscillation and deformation, N_{surf}, decreases due to the generation of small bubbles, and the breakup process may be governed by N_{surf} = min. The consequence of this tendency is that the local flow field is taken over by liquid phase. In contrast, when bubbles merge into a larger one, the energy dissipation through liquid turbulence, N_{turb}, may decrease and tends to minimum to favor the existence of large bubbles. The consequence of this tendency is the dominance of gas over the flow field. Thus, bubble coalescence and breakup reflects the dynamics of this compromising process, and the establishment of balance between breakup and coalescence may correspond to the solution of DBS model with a global minimum of $(N_{surf} + N_{turb})/N_T$.

It is generally accepted that the spectrum of flow regimes of gas−liquid flow starts from the bubbly flow where bubbles dispersed in continuous liquid at one extreme, then covers the slug flow, churn-turbulent flow, and annular flow, and ends with the mist flow where droplets dispersed in continuous gas. The existence of different regimes and their transition could be understood from the perspective of the concept of compromise. Unlike gas−solid flow, the interfacial instabilities of bubbles or droplets may also present as one of the dominant mechanisms in gas−liquid system. The two-phase flow is not only subject to the dominance of movement tendencies of the bulk of gas and liquid phases, but also influenced by the interfacial instabilities. Modeling interfacial instabilities needs further verification with experiments and microscale simulations.

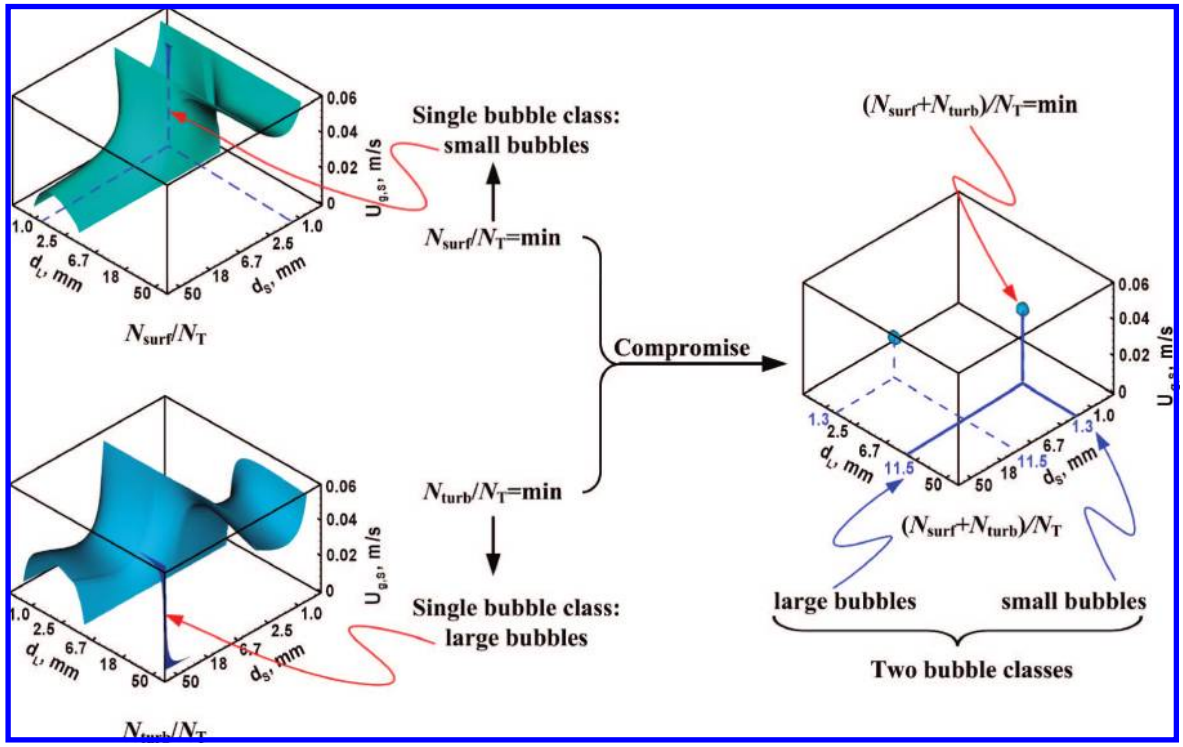

Figure 13. Contour plots of different energy consumption parts for $U_g = 0.06$ m/s.

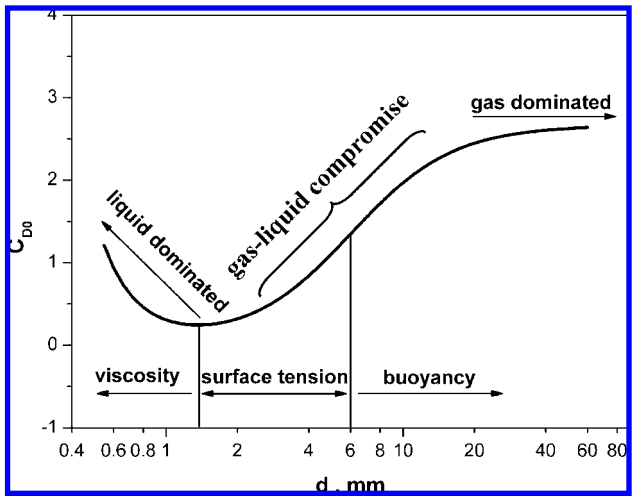

Figure 14. Compromise of the movement tendency for a single bubble.

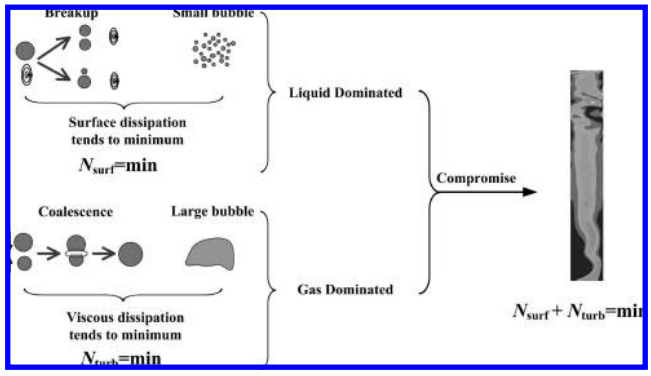

Figure 15. Relationship between the dynamics of compromise and the bubble coalescence and breakup.

7. Conclusions

Regime transition reflected by the jump change of a gas holdup curve in our previous calculation with the DBS model can be physically understood via the jump change of the location of global minimum of energy dissipated directly through microscopic interactions between two local minima. In this work, the jump change is further clarified through the exploration of the iso-surface of $(N_{surf} + N_{turb})/N_T$ and tracing the trajectory of the global minimum point in the three-dimensional space of structure parameters. It is this jump change which drives the variation of structural parameters and therefore gives rise to regime transition. The difference of the DBS model calculation with various drag coefficient correlations arises from the calculation of energy dissipation N_{surf} for small bubbles which is indispensable for characterizing the heterogeneous structure. The DBS model is also used for aqueous solution of saccharose and glycerin systems to investigate the influence of liquid viscosity. The model can reasonably predict the dual effect of liquid viscosity on regime transition reported in literature. Compared with a pure water system, a slight increase in viscosity stabilizes the homogeneous flow, which is reflected by the deferment of jump change in the calculation. Further increase to higher viscosity causes the advance of jump change, indicating the unfavorable effect of viscosity on the stability of homogeneous flow. Seeking the dominant mechanisms and analyzing their compromise is the key step for formulating the stability condition used to close the DBS model. This work also attempts to explore the dominant mechanisms for the motion of a single bubble, and the relation of the dynamics of compromise with bubble coalescence and breakup. The investigation of the dominant mechanisms and the stability condition may be of general relevance and significance to the fundamentals of multiphase flow and therefore need further extensive study.

Notation

C_{Db} = drag coefficient for a bubble in a swarm, dimensionless

$C_{D0,b}$ = drag coefficient for a bubble in a quiescent liquid, dimensionless

C_{Dp} = drag coefficient for a particle in multiparticle systems, dimensionless

$C_{D0,p}$ = drag coefficient for a particle in a quiescent fluid, dimensionless

c_f = coefficient of surface area increase, $c_f = f_{BV}^{2/3} + (1 - f_{BV})^{2/3} - 1$, dimensionless

d_b = bubble diameter, m

d_L = bubble diameter of large bubbles, m

d_{min} = minimum bubble diameter, mm

d_S = bubble diameter of small bubbles, m

Eo = Eötvös number, dimensionless

f_b = volume fraction of gas phase, dimensionless

f_L = volume fraction of large bubbles, dimensionless

f_S = volume fraction of small bubbles, dimensionless

f_{BV} = breakup ratio of daughter bubble to its mother bubble, dimensionless

g = gravitational acceleration, m/s^2

Mo = Morton number, dimensionless

N_{break} = rate of energy consumption due to bubble breakage per unit mass, m^2/s^3

N_{surf} = rate of energy dissipation due to bubble oscillation per unit mass, m^2/s^3

N_{turb} = rate of energy dissipation in turbulent liquid phase per unit mass, m^2/s^3

N_{st} = rate of energy dissipation for suspending and transporting particles per unit mass, m^2/s^3

n_b = number density of bubbles, 1/m^3

P_b = bubble breakup probability, dimensionless

U_g = superficial gas velocity, m/s

$U_{g,L}$ = superficial gas velocity for large bubbles, m/s

$U_{g,S}$ = superficial gas velocity for small bubbles, m/s

U_l = superficial liquid velocity, m/s

u_{slip} = slip velocity, m/s

U_T = terminal rise velocity, m/s

V_T = terminal rise velocity, m/s

W_{st} = rate of energy dissipation for suspending and transporting particles per unit volume, J/(m^3·s)

Greek Letters

ϵ = voidage, dimensionless

λ = character size of eddy, m

μ = viscosity, Pa·s

ρ = density, kg/m^3

σ = surface tension, N/m

ω = collision frequency, between eddy and bubble, 1/(m^4·s)

Abbreviations

DBS = dual-bubble-size

EMMS = energy-minimization multiscale

SBS = single-bubble-size

PHeR = pure heterogeneous regime

THeR = heterogeneous regime resulted from the instability of homogeneous regime

Subscripts

b = bubble

g = gas

L = large bubble

l = liquid

p = particle

S = small bubble

Acknowledgment

The long term support from the National Natural Science Foundation of China, in particular, Grant Nos. 20406022, 20221603, and 20490201, and the support from the Hi-tech Research and Development Program of China under Grant 2006AA030202, are gratefully acknowledged.

Literature Cited

(1) Fan, L.-S. *Gas-Liquid-Solid Fluidization Engineering*; Butterworth: Markham, ON, Canada, 1989.

(2) Deckwer, W. D. *Bubble Column Reactors*; Wiley: Chichester, U.K., 1992.

(3) Li, J.; Wen, L.; Qian, G.; Cui, H.; Kwauk, M.; Schouten, J. C.; Van den Bleek, C. M. Structure heterogeneity, regime multiplicity and nonlinear behavior in particle-fluid systems. *Chem. Eng. Sci.* **1996**, *51*, 2693–2698.

(4) Chen, R. C.; Reese, J.; Fan, L.-S. Flow structure in a three-dimensional bubble column and three-phase fluidized bed. *AIChE J.* **1994**, *40*, 1093–1104.

(5) Tzeng, J.-W.; Chen, R. C.; Fan, L. -S. Visualization of flow characteristics in a 2-D bubble column and three-phase fluidized bed. *AIChE J.* **1993**, *39*, 733–744.

(6) Zahradnik, J.; Fialova, M.; Ruzicka, M.; Drahos, J.; Kastanek, F.; Thomas, N. H. Duality of the gas-liquid flow regimes in bubble column reactors. *Chem. Eng. Sci.* **1997**, *52*, 3811–3826.

(7) Zahradnik, J.; Fialova, M. The effect of bubbling regime on gas and liquid phase mixing in bubble column reactors. *Chem. Eng. Sci.* **1996**, *51*, 2491–2500.

(8) Boyer, C.; Duquenne, A.-M.; Wild, G. Measuring techniques in gas-liquid and gas-liquid-solid reactors. *Chem. Eng. Sci.* **2002**, *57*, 3185–3215.

(9) Camarasa, E., C.; Vial, S.; Poncin, G.; Wild, N.; Midoux, J. Bouillard Influence of coalescence behaviour of the liquid and of gas sparging on hydrodynamics and bubble characteristics in a bubble column. *Chem. Eng. Process.* **1999**, *38*, 329–344.

(10) Fransolet, E.; Crine, M.; Marchot, P.; Toye, D. Analysis of gas holdup in bubble columns with non-Newtonian fluid using electrical resistance tomography and dynamic gas disengagement technique. *Chem. Eng. Sci.* **2005**, *60*, 6118–6123.

(11) Jin, H.; Yang, S.; Wang, M.; Williams, R. A. Measurement of gas holdup profiles in a gas liquid cocurrent bubble column using electrical resistance tomography. *Flow Meas. Instrum.* **2007**, *18*, 191–196.

(12) Fransolet, E.; Crine, M.; L'Homme, G.; Toye, D.; Marchot, P. Analysis of electrical resistance tomography measurements obtained on a bubble column. *Meas. Sci. Technol.* **2001**, *12*, 1055–1060.

(13) Warsito, W.; Fan, L. S. ECT imaging of three-phase fluidized bed based on three-phase capacitance model. *Chem. Eng. Sci.* **2003**, *58*, 823–832.

(14) Warsito, W.; Fan, L.-S. Dynamics of spiral bubble plume motion in the entrance region of bubble columns and three-phase fluidized beds using 3D ECT. *Chem. Eng. Sci.* **2005**, *60*, 6073–6084.

(15) Cassanello, M.; Larachi, F.; Kemoun, A.; Al-Dahhan, M. H.; Dudukovic, M. P. Inferring liquid chaotic dynamics in bubble columns using CARPT. *Chem. Eng. Sci.* **2001**, *56*, 6125–6134.

(16) Chen, J.; Kemoun, A.; Al-Dahhan, M. H.; Dudukovic, M. P.; Lee, D. J.; Fan, L.-S. Comparative hydrodynamics study in a bubble column using computer-automated radioactive particle tracking (CARPT)/computed tomography (CT) and particle image velocimetry (PIV). *Chem. Eng. Sci.* **1999**, *54*, 2199–2207.

(17) Fraguio, M. S.; Cassanello, M. C.; Larachi, F.; Limtrakul, S.; Dudukovic, M. Classifying flow regimes in three-phase fluidized beds from CARPT experiments. *Chem. Eng. Sci.* **2007**, *62*, 7523–7529.

(18) Delnoij, E.; Kuipers, J. A. M.; van Swaaij, W. P. M.; Westerweel, J. Measurement of gas-liquid two-phase flow in bubble columns using ensemble correlation PIV. *Chem. Eng. Sci.* **2000**, *55*, 3385–3395.

(19) Reese, J.; Fan, L.-S. Transient flow structure in the entrance region of a bubble column using particle image velocimetry. *Chem. Eng. Sci.* **1994**, *49*, 5623–5636.

(20) Sousa, R. G.; Pinto, A. M. F. R.; Campos, J. B.; L, M. Effect of gas expansion on the velocity of a Taylor bubble: PIV measurements. *Int. J. Multiphase Flow* **2006**, *32*, 1182–11903.

(21) Gladden, L. F.; Anadon, L. D.; Dunckley, C. P.; Mantle, M. D.; Sederman, A. J. Insights into gas-liquid-solid reactors obtained by magnetic resonance imaging. *Chem. Eng. Sci.* **2007**, *62*, 6969–6977.

(22) Olmos, E.; Gentric, C.; Poncin, S.; Midoux, N. Description of flow regime transitions in bubble columns via laser Doppler anemometry signals processing. *Chem. Eng. Sci.* **2003**, *58*, 1731–1742.

(23) Harteveld, W. K.; Mudde, R. F.; Van den Akker, H. E. A. Estimation of turbulence power spectra for bubbly flows from Laser Doppler Anemometry signals. *Chem. Eng. Sci.* **2005**, *60*, 6160–6168.

(24) Simonnet, M.; Gentric, C.; Olmos, E.; Midoux, N. Experimental determination of the drag coefficient in a swarm of bubbles. *Chem. Eng. Sci.* **2007**, *62*, 858–866.

(25) Ruzicka, M. C.; Zahradnik, J.; Drahos, J.; Thomas, N. H. Homogeneous-heterogeneous regime transition in bubble columns. *Chem. Eng. Sci.* **2001**, *56*, 4609–4626.

(26) Wallis, G. B. *One-dimensional Two-phase Flow*; McGraw-Hill: New York, USA, 1969.

(27) Zuber, N.; Findlay, J. A. Average volumetric concentration in two-phase flow systems. *Int. J. Heat Transfer* **1965**, *87*, 453–468.

(28) Joshi, J. B.; Deshpande, N. S.; Dinkar, M.; Phanikumar, D. V. Hydrodynamic Stability Of Multiphase Reactors. In *Advances in Chemical Engineering*; Academic Press: New York , 2001; Vol. 26, pp 1−130.

(29) Monahan, S. M.; Fox, R. O. Linear stability analysis of a two-fluid model for air-water bubble columns. *Chem. Eng. Sci.* **2007**, *62*, 3159–3177.

(30) Bhole, M. R.; Joshi, J. B. Stability analysis of bubble columns: Predictions for regime transition. *Chem. Eng. Sci.* **2005**, *60*, 4493–4507.

(31) Lucas, D.; Prasser, H. M.; Manera, A. Influence of the lift force on the stability of a bubble column. *Chem. Eng. Sci.* **2005**, *60*, 3609–3619.

(32) Monahan, S. M.; Vitankar, V. S.; Fox, R. O. CFD predictions for flow-regime transitions in bubble columns. *AIChE J.* **2005**, *51*, 1897–1923.

(33) Li, J.; Tung, Y.; Kwauk, M. Method of Energy Minimization in Multiscale Modeling of Particle Fluid Two-Phase Flow. In *Circulating Fluidized Bed Technology II*; Basu, P., Large, J. F., Eds. Pergamon Press: New York: 1988; pp 75−89.

(34) Li, J.; Kwauk, M. *Particle-Fluid Two-Phase Flow-The Energy-Minimization Multi-Scale Method*; Metallurgical Industry Press: Beijing, 1994.

(35) Li, J.; Cheng, C.; Zhang, Z.; Yuan, J.; Nemet, A.; Fett, F. N. The EMMS model - its application, development and updated concepts. *Chem. Eng. Sci.* **1999**, *54*, 5409–5425.

(36) Ge, W.; Li, J. Physical mapping of fluidization regimes-the EMMS approach. *Chem. Eng. Sci.* **2002**, *57*, 3993–4004.

(37) Ge, W.; Chen, F.; Gao, J.; Gao, S.; Huang, J.; Liu, X.; Ren, Y.; Sun, Q.; Wang, L.; Wang, W.; Yang, N.; Zhang, J.; Zhao, H.; Zhou, G.; Li, J. Analytical multi-scale method for multi-phase complex systems in process engineering-Bridging reductionism and holism. *Chem. Eng. Sci.* **2007**, *62*, 3346–3377.

(38) Zhao, H. *Multi-scale modeling of gas-liquid (slurry) reactors. Ph.D. Thesis, Institute of Process Engineering*, Chinese Academy of Sciences, Beijing, 2006.

(39) Yang, N.; Chen, J.; Zhao, H.; Ge, W.; Li, J. Explorations on the multi-scale flow structure and stability condition in bubble columns. *Chem. Eng. Sci.* **2007**, *62*, 6978–6991.

(40) De Swart, J. W. A.; van Vliet, R. E.; Krishna, R. Size, structure and dynamics of "large" bubbles in a two-dimensional slurry bubble column. *Chem. Eng. Sci.* **1996**, *51*, 4619–4629.

(41) Krishna, R.; Ellenberger, J. Gas holdup in bubble column reactors operating in the churn-turbulent flow regime. *AIChE J.* **1996**, *42*, 2627–2634.

(42) Ribeiro, C. P.; Lage, P. L. C. Direct-contact evaporation in the homogeneous and heterogeneous bubbling regimes. Part II: dynamic simulation. *Int. J. Heat Mass Transfer* **2004**, *47*, 3841–3854.

(43) Tomiyama, A. Struggle with computational bubble dynamics. *Multiphase Sci. Technol.* **1998**, *10*, 369–405.

(44) Grace, J. R.; Wairegi, T.; Nguyen, T. H. Shapes and velocities of single drops and bubbles moving freely through immiscible liquids. *Trans. Inst. Chem. Eng.* **1976**, *54*, 167–173.

(45) Kulkarni, A. A.; Joshi, J. B. Bubble Formation and Bubble Rise Velocity in Gas-Liquid Systems: A Review. *Ind. Eng. Chem. Res.* **2005**, *44*, 5873–5931.

(46) Mendelson, H., D. The prediction of bubble terminal velocities from wave theory. *AIChE J.* **1967**, *13*, 250–253.

(47) Fan, L.-S.; Tsuchiya, K. *Bubble Wake Dynamics in Liquids and Liquid−Solid Suspensions*; Butterworth-Heinemann: Stoneham, 1990.

(48) Clift, R.; Grace, J. R.; Weber, M. E. *Bubbles, Drops, and Particles*; Academic Press: London, 1978.

(49) Snape, J. B.; Zahradnik, J.; Fialova, M.; Thomas, N. H. Liquid-phase properties and sparger design effects in an external-loop airlift reactor. *Chem. Eng. Sci.* **1995**, *50*, 3175–3186.

(50) Kazakis, N. A.; Mouza, A. A.; Paras, S. V. Experimental study of bubble formation at metal porous spargers: Effect of liquid properties and sparger characteristics on the initial bubble size distribution. *Chem. Eng. J.* **2008**, *137*, 265–281.

(51) Mouza, A. A.; Dalakoglou, G. K.; Paras, S. V. Effect of liquid properties on the performance of bubble column reactors with fine pore spargers. *Chem. Eng. Sci.* **2005**, *60*, 1465–1475.

(52) Ruzicka, M. C.; Drahos, J.; Mena, P. C.; Teixeira, J. A. Effect of viscosity on homogeneous-heterogeneous flow regime transition in bubble columns. *Chem. Eng. J.* **2003**, *96*, 15–22.

(53) Li, J.; Zhang, J.; Ge, W.; Liu, X. Multi-scale methodology for complex systems. *Chem. Eng. Sci.* **2004**, *59*, 1687–1700.

(54) Yang, G. Q.; Du, B.; Fan, L.-S. Bubble formation and dynamics in gas-liquid-solid fluidization-A review. *Chem. Eng. Sci.* **2007**, *62*, 2–27.

(55) Sanada, T.; Shirota, M.; Watanabe, M. Bubble wake visualization by using photochromic dye. *Chem. Eng. Sci.* **2007**, *62*, 7264–7273.

(56) Chen, P.; Sanyal, J.; Dudukovic, M. P. Numerical simulation of bubble columns flows: effect of different breakup and coalescence closures. *Chem. Eng. Sci.* **2005**, *60*, 1085–1101.

(57) Wang, T.; Wang, J.; Jin, Y. Theoretical prediction of flow regime transition in bubble columns by the population balance model. *Chem. Eng. Sci.* **2005**, *60*, 6199–6209.

Received for review March 5, 2008
Revised manuscript received May 26, 2008
Accepted May 29, 2008

IE8003623